Can Learning from Demonstration Approaches Encode and Generalise Human Movements for Neurorehabilitation?

Jia Quan Loh, Vincent Crocher, Denny Oetomo, Ying Tan

***Abstract*—The use of robotic systems in Upper-Limb (UL) neurorehabilitation typically involves semi-standardised, simple movement exercises controlled by the robot. However, alternative approaches aim to support more complex movements that align with Activities of Daily Living (ADLs) and offer greater customisation of interactions tailored to individual patients by clinicians. These approaches, however, require increased therapist involvement, which underscores the need for methods that allow clinicians to teach a set of exercises to the robot. This has led to the development of various Learning by Demonstration (LfD) algorithms. These algorithms require the ability to encode the movements demonstrated by the clinician and generalise them across various task variations. Towards this goal, this study compares two existing LfD algorithms, Task-Parameterised Gaussian mixture models (TPGMM) and Dynamic Movement Primitives (DMP), in their capacity to generalise UL movements required for ADLs. The study then extends the best performing algorithm — TPGMM — to encode movements from both healthy and post-stroke participants performing a drinking task. TPGMM shows better performance in generalising healthy human movements for tasks and environments of increasing complexity when compared to a model-based approach and DMPs. TPGMM further shows that it better encodes movements of individuals post-stroke compared to ones of healthy individuals.**

***Index Terms*—Neurorehabilitation, Upper-Limb, Learning from Demonstration, Generalisation, Movement Quality.**

I. Introduction

Although rehabilitation robotic approaches in Upper-Limb (UL) therapy often aim for a high-level of automation and standardisation of therapy [1], another approach consists of enabling the clinician to customise rehabilitation exercises and possibly orient patients towards more functional practice. In this later approach, as attempted by Johnson or Timmermans with the Haptic Master [2], [3] or by the authors [4], the robotic device is used as an adjunct for clinicians to provide high intensity and consistent feedback to the patient. Thus, the presence of the therapist is required at all times to redemonstrate movement when task variations are introduced, which in turn leads to decreased robot autonomy and limits the possible cost and intensity benefit of robots.

In this scenario, it is thus desirable to allow a clinician to demonstrate examples of a (potentially complex) rehabilitation exercise, customised to a given patient, and allow the robot to guide the patient through this exercise and associated variations in the next therapy episode. It is expected that the robot can capture the "essence" of the exercise demonstrated — and the associated therapist action — and that the robot can then autonomously guide the patient through the exercise and its variations.

The *encoding*, *reproduction* and *generalisation* of an action — or a set of actions — demonstrated by a user to a robot is the objective of Learning from Demonstration (LfD) approaches encountered in classic robotic applications including pick-and-place or complex object manipulation [5], [6].

In a neurorehabilitation scenario, we assume that the patient's movements are more important than the robot's, shifting the focus towards learning actual human movement. This requires LfD algorithms to be applied in a larger dimensional space representing UL joints compared to the 3-DoF wrist position or robot joints classically used in LfD. The learning can then be extended towards human-on-human demonstration during therapy rather than relying on the rehabilitation robot's parameters during kinaesthetic teaching.

Reviewing existing literature on LfD in neurorehabilitation, Najafi et al. [7], Luciani et al. [8] and Lauretti et al. [9] employed Gaussian Mixture Models (GMM), Hidden Markov Models and Dynamic Movement Primitives (DMP) respectively to encode the joint kinematics of rehabilitation robots.

Noticeably, most LfD approaches constrain their learning space within the robot parameters, though one could argue that [8], [9] provides an UL approximation using their exoskeleton. Only Liu et al. [10] attempted to encode actual UL joints of humans using Kernel Movement Primitives. Furthermore, only [9] thoroughly evaluated the generalisability of deterministic LfD algorithms to tasks variations (*i.e.* new task points), which is essential to quantify the level of autonomy a rehabilitation robot can achieve. More importantly, to date, only [11] proposed a formal comparison of human movement quality preserved from each algorithm's reconstruction.

In this work, we extend Luciani's work [11] by investigating how well existing LfD algorithms generalise UL movement for unimanual daily activities (*e.g.* pick-place and drinking tasks) used in rehabilitation sessions. Specifically, this work proposes implementations of Task-Parameterised Gaussian Mixture Models (TPGMM) and DMP applied to UL joint trajectories (see Section II) and compares their performances on experimental data to a purely model-based representation of UL kinematics (using minimum jerk trajectories and inverse kinematics). The comparison is specifically evaluated on

The authors are with the Human Robotics Laboratory, Department of Mechanical Engineering and the Graeme Clark Institute, The University of Melbourne.
Correspondence: jqloh@student.unimelb.edu.au

kinematic metrics relevant to human movement analysis and rehabilitation (see Section III). In addition, we tested whether the best performing algorithm is able to capture the specificity of the movements of stroke patients compared to those of people without impairment for a classic drinking task from an existing datatset [12].

II. Objective and LfD algorithms evaluated

A. Upper-limb kinematics modelling and encoding objective

In this work, we propose to compare how well existing LfD algorithms are able to encode UL joint trajectories for common ADLs and generalise these trajectories to task variations (*i.e.* different starting, final or intermediate — via — points). Due to the importance of varying task points, we chose algorithms that explicitly address varying task points within their mathematical formulation to ensure convergence towards specified points.

The UL is modelled as a two links serial manipulator, connected with four DoFs: three coaxial revolute joints representing the gleno-humeral joint and a revolute joint for the elbow flexion-extension. This model references the MVN Biomechanical model for ease of comparison with datasets captured using XSENS (Xsens Technologies, Enschede, Netherlands).

B. LfD algorithms evaluated

The objective of the LfD algorithms is to encode a demonstrated kinematic trajectory $\Xi \in \mathcal{R}^{T\times 5}$, made of T vectors $\boldsymbol{\xi}_t = [\sigma_t, q_{1,t}, q_{2,t}, q_{3,t}, q_{4,t}]$ with $q_{1-4,t}$ the UL joint angles and σ_t the sampled time at each timestep $t \in [1, \ldots, T]$.

Both TPGMM and DMP algorithms are adapted as follows to encode UL joint movements rather than the conventional task space movement.

1) Task-Parameterised Gaussian Mixture Model and Regression (TPGMM + GMR): In contrast to stochastic policies (*e.g.* ProMPs, HMM) that generalise distributions in a single reference frame (*e.g.* inertial frame or the trajectory starting point or end point), TPGMM adapts the distribution to multiple different start, final or via-points by superposing different reference frames relevant for a task [13].

For each task demonstration, the joint trajectory Ξ is observed from P reference frames, each assigned to the start, via and final points of the demonstration. Each p^{th} reference frame is characterised by a rotation matrix $A_p \in \mathcal{R}^{N\times N}$ and a displacement vector $\boldsymbol{b}_p \in \mathcal{R}^{1\times 5}$, referenced from an inertial frame. The kinematic profile at time step t in the p^{th} reference frame, denoted as $\boldsymbol{\xi}_t^{(p)}$, can be expressed as

$$\boldsymbol{\xi}_t^{(p)} = A_p^{-1}(\boldsymbol{\xi}_t - \boldsymbol{b}_p), \quad p = 1, ..., P, \tag{1}$$

where $\boldsymbol{\xi}_t$ is the t^{th} row vector of Ξ. Adapting this to joint space, A_p is set to the identity matrix and $\boldsymbol{b}_p$ is the joint displacement from the origin pose when the UL is at the p^{th} reference frame. Here, the displacement $\boldsymbol{b}_p$ represents the full transformation from one reference UL posture to another.

M demonstrations of P trajectories with T time steps each are concatenated demonstration by demonstration.

From these observations, K Gaussian kernels are identified, with each k^{th} kernel parameterised to P multivariate Gaussian distributions $\mathcal{N}(\boldsymbol{\mu}_k^{(p)}, \Sigma_k^{(p)})$ and their associated weight π_k. $\boldsymbol{\mu}_k^{(p)}$ and $\Sigma_k^{(p)}$ are respectively the mean vector and covariance matrix of the k^{th} Gaussian kernel in the p^{th} reference frame.

The number of Gaussian kernels K required to represent the task is optimised using the Bayesian Information Criterion test [14]. The $\boldsymbol{\mu}_k^{(p)}$ and $\Sigma_k^{(p)}$ of each Gaussian distribution are identified by an Expectation-Maximisation algorithm which maximises the likelihood of the demonstrated trajectories to lie within the identified Gaussian distributions [13].

To reconstruct a movement for new start, via and final UL postures, a new GMM and its corresponding Gaussian kernels $\mathcal{N}(\hat{\boldsymbol{\mu}}_k, \hat{\Sigma}_k)$ is obtained by conditioning the learned $\mathcal{N}(\boldsymbol{\mu}_k^{(p)}, \Sigma_k^{(p)})$ to the new reference frames defined by $\boldsymbol{b}_p$ (*i.e.* the joint configurations required at the new task points):

$$\hat{\boldsymbol{\mu}}_k = \Sigma_k \sum_{p=1}^{P} \Sigma_k^{(p)^{-1}} \hat{\boldsymbol{\mu}}_k^{(p)}, \quad \hat{\Sigma}_k = \left(\sum_{p=1}^{P} \Sigma_k^{(p)^{-1}}\right)^{-1} with \tag{2}$$

$$\hat{\boldsymbol{\mu}}_k^{(p)} = \boldsymbol{\mu}_k^{(p)} + \boldsymbol{b}_p. \tag{3}$$

The conditioned GMM is then used to generate a new motion plan with the sampled time, σ_t as the input, via Gaussian Mixture Regression, which calculates the conditional probability and expectation of the output for this given input.

Note: The conditioning of the new GMM (Eq. 2 and 3) is simplified compared to the common $\mathcal{R}^3$ case given the absence of rotation A_p in the joint configuration space.

2) Dynamic Movement Primitives: Dynamic Movement Primitives formulate a movement as a dynamical model (*e.g.* a spring-damper system) that modulates its non-linear forcing term after a desired attractor behaviour, usually an ideal demonstrated trajectory [15]. For each DoF of the UL model, the equation of the point attractor system is given by:

$$\tau \ddot{q}_n(t) = \alpha_n(\beta_n(g_n - q_n(t)) - \dot{q}_n(t)) + f_n(x), \tag{4}$$

where $q_n(t)$, $\dot{q}_n(t)$ and $\ddot{q}_n(t)$ are the n^{th}-DoF trajectory and its time derivatives, τ is the duration of the demonstrated movement and $g_n = q_n(t = \tau)$ is the corresponding joint angle of the final UL posture. α_n and β_n are positive constants selected such that the system is critically damped (*e.g.* $\beta_n = \alpha_n/4$). $f_n(x)$ is the forcing term expressed as:

$$f_n(x) = \frac{\sum_{k=1}^{K} \Psi_k(x_n)\omega_k}{\sum_{k=1}^{K} \Psi_k(x_n)} x_n(g_n - s_n), \tag{5}$$

where K is the chosen number of Gaussian kernels, $s_n = q_n(t = 0)$ is the starting posture of the trajectory, and ω_k are the DMP weights that will be learned from the demonstration(s) [15]. $\Psi_k(x_n)$ are Gaussian kernels expressed as:

$$\Psi_k(x_n) = \exp\left(-\frac{1}{2\sigma_k^2}(x_n - \mu_k)^2\right), \tag{6}$$

where σ_k and μ_k are the selected widths and centers of the Gaussian kernels.

(5) and (6) are dependent on state variable x_n, expressed as a decaying canonical system to inhibit time dependence of the system:

$$\tau \dot{x}_n = -\gamma_n x_n, \tag{7}$$

where γ_n is set as a positive constant. Recommended values for α_n, μ_k, σ_k and γ_n were obtained from [16]. As there are no formal optimisation process for the exact number of K, a linear search up to 250 kernels was performed, with K kernels providing lowest RMSE when reconstructing the training dataset.

DMP weights ω_k are learned through the Locally Weighted Regression algorithm [17]. Given a demonstration of T time steps indexed by $t \in [1, ..., T]$, the recorded DoF and their derivatives, $q_n(t)$, $\dot{q}_n(t)$ and $\ddot{q}_n(t)$, are inserted into (4) to obtain T forcing terms f_n at each timestep:

$$f_n(t) = \tau \ddot{q}_n(t) - \alpha_n(\beta_n(g_n - q_n(t)) - \dot{q}_n(t)). \tag{8}$$

To learn ω_k, the locally weighted quadratic error is minimised for each Gaussian kernel using the following cost function, J_k:

$$J_k = \sum_{t=1}^{T} \Psi_k(x)(f_n(t) - \omega_k \epsilon(x))^2 \quad with \tag{9}$$

$$\epsilon(x) = x_n(t)(g_n - s_n). \tag{10}$$

An independent DMP is learned for each DoF of the UL model. As proposed by Lauretti et al. [9] to overcome the potential limitation of encoding a complex task with a single set of DMPs, a task is divided into sub-movements (each corresponding to a part of the movement stopping at a via-point and with a zero-velocity crossing) for which the above DMP approach is applied, effectively creating a dictionary of DMPs for different sub-movements. To reconstruct each new sub-movement, the start and final posture, s_n and g_n are adjusted to the desired postures and inserted into (4) and (5) of the corresponding DMP for said sub-movement. The q_n trajectory is obtained via forward integration.

Given the DMP approach does not explicitly learn from multiple demonstrations; when required, the ideal learning trajectory is taken from the average of multiple demonstrations aligned in time.

3) Model-based comparison: In addition to the two LfD algorithms above, a purely model-based approach is used as a comparison point in this work. Namely, the hand trajectory for each sub-movement is represented by a point-to-point minimum jerk function [18].

A numerical inverse kinematics using the Moore-Penrose inverse and Gauss-Newton algorithm is then applied onto each sampling point to define the corresponding UL posture. For the first point of each sub-movement the actual UL posture is used as the initial guess of the optimisation.

The joint space trajectories obtained with this model-based methods are then evaluated the same way as the trajectories obtained from the LfD algorithms.

III. Experimental evaluations

Two distinct experimental evaluations of these LfD algorithms were performed to evaluate if these methods could be used in neurorehabilitation: one to assess the ability of LfD algorithms to generalise healthy human movements to new task variations; and a second one to evaluate if the best of these algorithms can encode the specificity of participants with UL impairment after stroke. Both experiments rely on the evaluation of reconstructed movements (by LfD algorithms and model) against the original human movements. This comparison is here performed thanks to dedicated kinematic metrics.

A. Evaluation metrics and analysis

The set of metrics selected aims to cover the human likeness aspect of movements both at the end-effector and joints level and their temporal and spatial aspects:

1) *Joints Trajectory Dynamic Time Warping (Joints DTW)*: DTW aligns two signals by optimizing the distance value between points of the signals at current and previous time steps [19]. Its associated alignment cost is used as a temporal similarity measure for human action recognition [20]. DTW is used to evaluate the temporal similarity of the UL joints trajectories.
2) *Swivel Angle Trajectory DTW (Swivel DTW)*: Considering a 4-DoF UL model, a reaching movement contains a redundant DoF which can be parameterised by the swivel angle [21]. The swivel angle is defined as the angle between the the arm-plane and the vertical direction, with 0° when the arm-plane is parallel to the sagittal plane and 90° when parallel to the transverse plane. DTW is applied separately to the swivel angle trajectory to evaluate similarity of the encoded movement's redundancy.
3) *Mean Absolute Relative Phase Difference ($\Delta MARP$)*: Continuous Relative Phase (CRP) quantifies inter-joint coordination. It extracts phase angles between joint position and velocity, then compares it between different joints. A joint trajectory, $q(t)$ is decomposed into a complex signal, $\zeta(t)$ using the Hilbert Transform, $H(q(t))$ as described in [22]:

$$\zeta(t) = H(q(t)) = q(t) + iH(t). \tag{11}$$

The phase trajectory $\phi(t)$ is calculated by

$$\phi(t) = \arctan\left(\frac{H(t)}{q(t)}\right). \tag{12}$$

The CRP trajectory, $CRP(t)$ between two joints $q_1(t)$ and $q_2(t)$ is obtained by subtracting the phase angles

$$CRP(t) = \phi_1(t) - \phi_2(t). \tag{13}$$

where $\phi_1(t)$ and $\phi_2(t)$ is the phase angles of the two joints respectively.

Since CRP is a time series, the mean absolute value over the trajectory called Mean Absolute Relative Phase (MARP) is used to quantify the average phase of a movement [23]. To capture the extent of how the LfD algorithms encode joints coordination, the maximum difference in MARP between movements is reported in this study (*i.e.* the worst change among the six inter-joint pairs).

4) *Hand Trajectory Hausdorff Distance (Hand HD)*: The minimum Hausdorff Distance is the minimum value of the greatest of all the distances from a point in one trajectory to the closest point in the other trajectory [24]. HD is used to evaluate spatial similarity between hand movements, independently of time.
5) *Smoothness Difference (ΔSAL)*: Spectral Arc Length (SAL) defines movement smoothness as introduced in [25]. SAL is always negative with a value closer to zero corresponding to a smoother movement. The difference ΔSAL between the SAL of recorded and reconstructed sub-movements is calculated.
6) *Time-to-Peak-Speed Difference (ΔTTP)*: The speed profile of each sub-movement is calculated on the hand trajectory using a first-order Euler approximation. The peak speed and time-to-peak-speed refer to the largest value in the profile and corresponding time stamp relative to the start of the sub-movement. For each sub-movement, TTP is normalised to the sub-movement duration [26] and the difference ΔTTP between these normalised TTP is calculated. The average ΔTTP across all sub-movements is reported.

For all these metrics, a smaller value corresponds to a better, more faithful, movement reconstruction.

B. Experiment 1 - Standardised ADLs generalisation

In the first experiment, participants without movement impairment were recruited to perform ADLs tasks. The study was approved by the University of Melbourne HREC ($\#2024-31144-60078-3$).

1) Setup: Participant's joint angles were recorded using Vive Inertial Trackers (HTC, Taiwan) providing 6-DoF position and orientation measurements at the shoulder, the end of the humerus, and the wrist as shown on Fig. 1-a and recording at 90Hz. The trackers are interfaced with a custom C# program and a Unity UI (Unity Technologies, USA).

2) Task protocol: Participants were asked to sit at a table in front of a custom setup (see Fig. 1-b) and to perform a series of physical tasks while wearing the Vive Trackers.

Four tasks of increasing complexity associated with ADLs were selected: T1-Planar Pick-Place, T2-Elevated Pick-Place, T3-Obstructed Planar Pick-Place and T4-Pick-Drink. For each task, six configurations corresponding to a different picking or placing locations were recorded (see Fig. 2 and Table I). The placement of the task points were normalised based on the participant's forearm length, shoulder width and furthest diagonal reach.

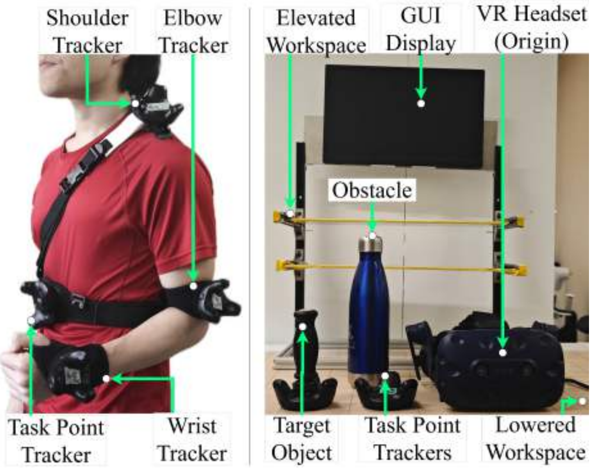

Fig. 1. Motion capture sensors (a) and experimental bench (b) and used for standardised ADLs movements recording. Note that the VR headset is only used here as a reference frame and not worn by the participants.

TABLE I
TASK DESCRIPTION

Task	Sub-task	Description
1	1-1	Move wrist from home position to TP1.
	1-2	Move object from TP1 to TP2 on a low level.
	1-3	Release object on TP2 and return to home position.
2	2-1	Move wrist from home position to TP1.
	2-2	Move object from TP1 to TP2 on an elevated level.
	2-3	Release object on TP2 and return to home position.
3	3-1	Move wrist from home position to TP1.
	3-2	Move object from TP1 to TP2 on a low level avoiding the obstacle in the middle.
	3-3	Release object on TP2 and return to home position.
4	4-1	Move wrist from home position to TP1.
	4-2	Move object from TP1 to mouth.
	4-3	Return to home position.

For each task, participants were asked to perform three demonstrations for each configuration using their dominant hand. They were then given a ten-minute rest, before repeating the experiment with their non-dominant hand. The overall session consisted in a total of 144 tasks repetitions.

3) Data post-processing and analysis: A fourth-order, low-pass Butter-worth filter with a cut-off frequency of 5Hz [27] was applied on joint angle signals. The filtered signal is then down-sampled to 50Hz to reduce model computation. To align multiple demonstrations in time, each joint trajectory was then normalised to unit time.

For each Task and each Participant, two non contiguous configurations were randomly selected for generalisation evaluation whereas the remaining four configurations were used for LfD training. The reconstructed trajectories from the generalisation set were compared to their corresponding recorded movements using the six kinematic metrics.

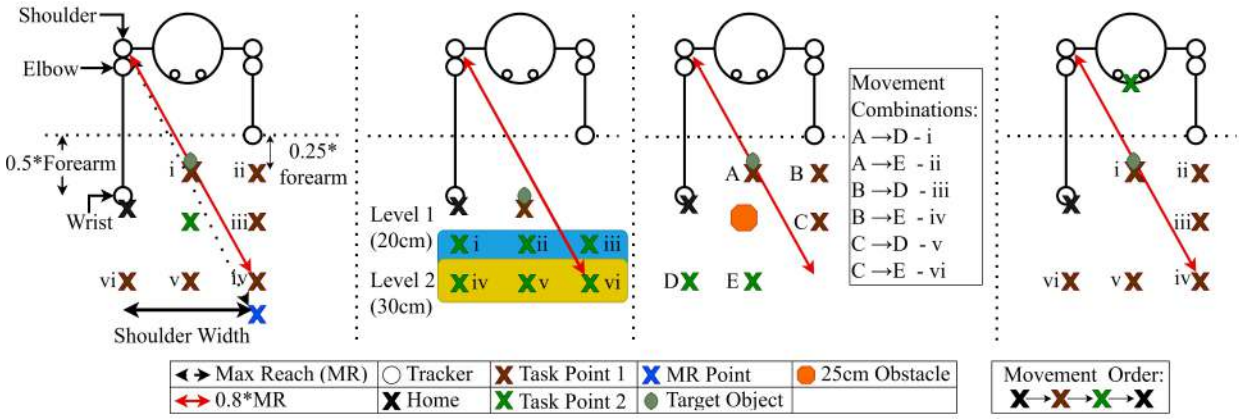

Fig. 2. Schematic of setup and Tasks configurations $i - vi$. Overall motion consists of moving from the home position (black cross) to grasp the object at TP1 (red cross), transporting it to TP2 (green cross) and returning to the home position. From left to right: 1) Lowered Pick-Place, 2) Elevated Pick-Place, 3) Obstructed Pick-Place, 4) Pick-Drink.

Distribution of each metric outcome for each LfD Algorithm and each Task were tested for normality (Shapiro–Wilk test, $p < 0.05$), followed by a repeated ANOVA / Friedman test and corresponding post-hoc paired t-test / Wilcoxon signed-rank test to evaluate differences between the three reconstructions.

C. Experiment 2 - Impaired movements encoding

To further evaluate the capability of LfD algorithms to encode movements for a rehabilitation context, the best performing algorithm was further applied to encode movements of five participants with stroke (51 to 74 years, FMA-UE: 21 to 61) and five control healthy participants (42 to 78 years) performing a drinking task. Movements were selected from the UL-ADL dataset by Schwarz et al. [12]. Only participants with a right-dominant-impaired side were selected for better comparison with the group of non-impaired individuals (all right handed). TPGMM as described in Section II was used to encode each task for each participant (using three repetitions).

Movement reconstructions were then compared to the three recorded repetitions using the same set of kinematic metrics. The distribution of the metrics difference for each group are reported for comparison.

This analysis specifically aims to test if the encoding of movements preserve the specificity of movements with participants with stroke compared to the encoding of individuals without neurological injury (*i.e.* are movements of individuals with stroke reconstructed as well or worse as those of healthy individuals).

IV. RESULTS

A. Experiment 1 - Standardised ADLs generalisation

Five naive, healthy participants (28.4 ± 3.36 years old) were recruited. According to the Edinburgh Handedness Inventory [28], three participants were predominantly right-handed, 1 ambidextrous, and 1 predominantly left-handed.

Fig. 3 shows an example of an Obstructed Pick-place task (Task 3) and corresponding reconstruction by the LfD algorithms.

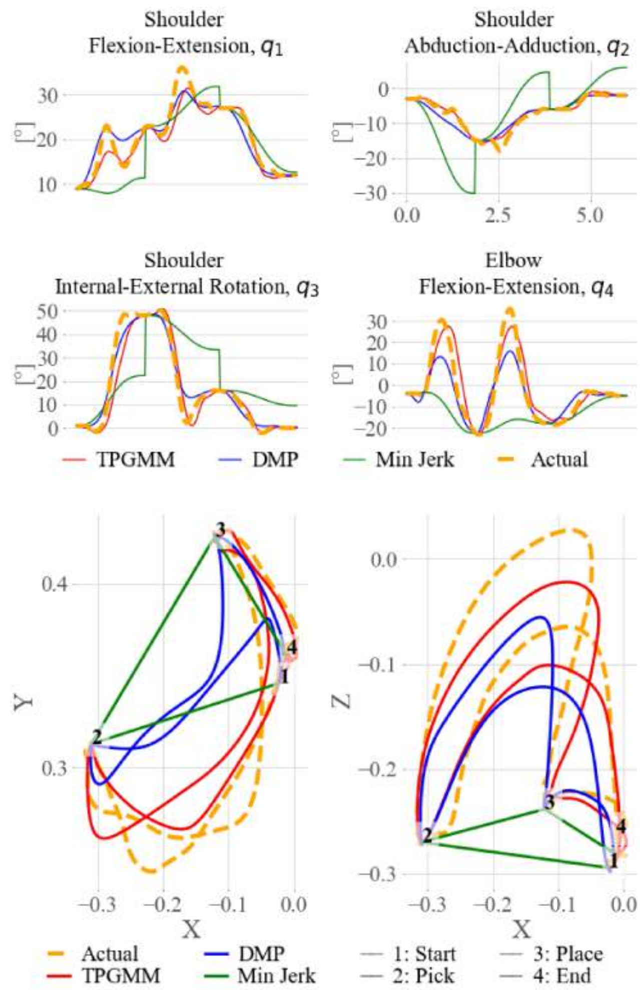

Fig. 3. Example of actual and reconstructed UL joint trajectories (a) and hand trajectories (b) (left: Top View, Right: Front View) between actual and reconstructed joints for Task 3 - Obstructed pick-place task.

Table II presents the mean difference (and post-hoc significance level) between the different approaches for each metric for each task. Metrics for which methods are not statistically different are omitted.

TABLE II
METRIC COMPARISON BETWEEN LFD ALGORITHMS AND MINIMUM JERK

Metric	Mean Difference $i - j$			Best
	TPGMM -Min Jerk	DMP -Min Jerk	TPGMM -DMP	
Task 1 – Planar Pick-Place				
Joints DTW (rad)	-1.807***	-1.743***	-	-
Swivel DTW (rad)	-0.231***	-0.219***	-	-
ΔMARP	-0.106**	-	-	-
Hand HD (m)	-0.018*	-	-	-
ΔSAL	-	-	-	-
ΔTTP	-	-	-	-
Task 2 – Elevated Pick-Place				
Joints DTW (rad)	-3.695***	-3.850***	-	-
Swivel DTW (rad)	-0.681**	-0.719**	-	-
ΔMARP	-0.194**	-0.209**	-	-
Hand HD (m)	-0.075***	-0.077***	-	-
ΔSAL	-0.364***	-0.393***	-	-
ΔTTP	-0.033*	-0.076***	0.043***	DMP
Task 3 – Obstructed Pick-Place				
Joints DTW (rad)	-3.150***	-2.244***	-0.906***	TPGMM
Swivel DTW (rad)	-0.369***	-0.236**	-0.133**	TPGMM
ΔMARP	-0.247**	-0.124*	-	-
Hand HD (m)	-0.056**	-0.023**	-0.033**	TPGMM
ΔSAL	-	-	-	-
ΔTTP	-	-0.061***	0.037*	DMP
Task 4 – Pick-Drink				
Joints DTW (rad)	-5.855***	-5.857***	-	-
Swivel DTW (rad)	-	-	-	-
ΔMARP	-0.232***	-0.192*	-	-
Hand HD (m)	-0.056***	-0.043***	-0.013*	TPGMM
ΔSAL	-0.404*	-0.333*	-	-
ΔTTP	-0.056**	-0.095***	0.039*	DMP

$^{*}p < 0.05$, $^{**}p < 0.01$, $^{***}p < 0.001$.

B. Experiment 2 - Impaired movements encoding

Fig. 4 compares the distribution of the metrics obtained from TPGMM reproductions between healthy and post-stroke participants.

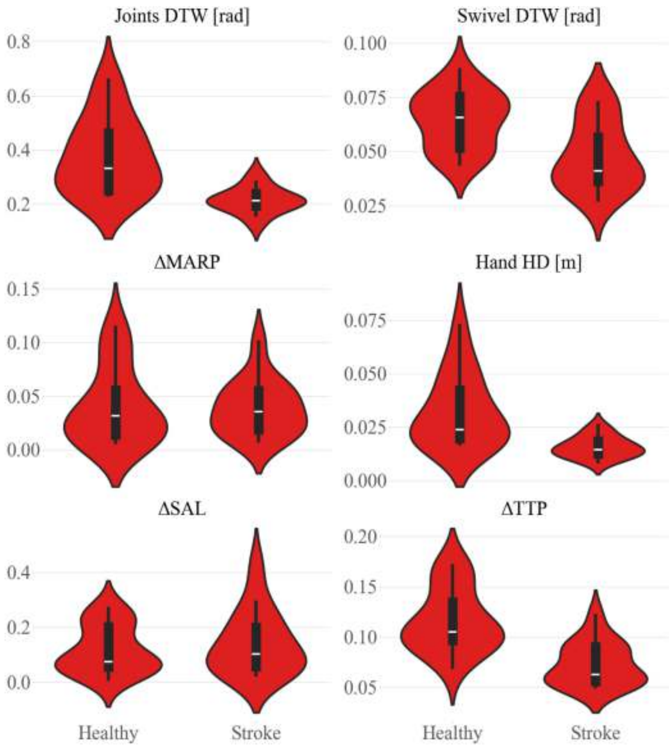

Fig. 4. Violin plots showing the metric distribution of TPGMM reconstruction for healthy and stroke participants.

V. DISCUSSION

A. Generalisation over increasing task complexity

The purely model-based approach is able to generate simple planar point-to-point movements of the hand equally well to the LfD policies but already failed to capture as good a representation in joints space. As task complexity increases and divert from a simple point-to-point reaching, the LfD algorithms perform significantly better than the simple model, even in reproducing the hand trajectory.

Although DMPs and TPGMM did not show significant difference in maintaining human likeness for its generalisation during T1, T2 and T4; of which a similar behaviour was observed in [11]'s work for reproducing pick-place and pick-drink joint movement; TPGMM significantly better generalises to new task parameters than DMPs when both task and environment becomes more complex, demonstrated by the addition of obstacles in T3. While not visible for all metrics, this is clear for both hand space (as shown by the Hand HD) and joints space (as shown by the Joints DTW and Swivel angle DTW) for T3 as presented on Table II. This better generalisation of complex tasks might be due to TPGMM's formulation that explicitly observes the joints distribution from multiple coordinate frames.

Importantly, the advantage of TPGMM is clearly visible in joint space (Joints and Swivel DTW). This is an important point for neuro-rehabilitation given the specificity of joint synergies and compensatory behaviour observed post-stroke which are desirable to capture.

In addition, the complexity (*i.e.* number of kernels) of LfD techniques can significantly influence their performance and, despite using optimisations approaches in this work, the choice made may have influenced the results. Still, it is to note that TPGMM outperforms DMPs in the current work while requiring a lower number of kernels with 118 on average compared to 280 for DMPs.

B. Encoding of movements specificity of participants with stroke

It is well documented that following a stroke, UL movements are impaired and the execution of classic tasks differs in multiple way from one of healthy individuals. Thus, evaluating how TPGMM, which shows the best ability in more complex tasks, can capture this specificity does provide an indication on how well it could encode rehabilitation movements (*i.e.* assuming that those movements lie somewhere in between those of healthy individuals and natural ones of the stroke patient). Interestingly, the evaluation performed on a drinking task reveals that TPGMM produces a more faithful and consistent encoding of stroke participants' movements compared to ones of healthy individuals. This is the case for all metrics except for ΔSAL (see Fig. 4). This encoding performance comes at the expense of an increased modelling complexity: healthy participants movements required between 20 and 63 kernels, whereas stroke participants movements required between 38 and 92 kernels.

C. Limitations and future work

It is to note that the UL model used is limited to only four DoFs and does not include any scapula or trunk motion. This is an important limitation for rehabilitation applications where patients tend to compensate for limited elbow and shoulder flexion/extension using trunk and scapula motions [29]. Such motions should thus ideally be encoded and reconstructed by the LfD policies.

While this first analysis provides insights on the two LfD algorithms to encode human movements that could be used in neurorehabilitation, the two experiments presented do not truly represent actual rehabilitation exercise prescribed by therapists. While the results indicate that TPGMM is the best candidate for such scenario, a formal evaluation in real conditions should still be conducted.

Acknowledgement

This work was supported by the Australian Research Council (#LP220100417).

References

[1] P. J. Mahdieh Babaiasl, Seyyed Hamed Mahdioun and M. Yazdani, "A review of technological and clinical aspects of robot-aided rehabilitation of upper-extremity after stroke," *Disability and Rehabilitation: Assistive Technology*, vol. 11, no. 4, pp. 263–280, 2016.

[2] M. Johnson, K. Wisneski, J. Anderson, D. Nathan, and R. Smith, "Development of ADLER: The Activities of Daily Living Exercise Robot," in *The First IEEE/RAS-EMBS International Conference on Biomedical Robotics and Biomechatronics*, 2006, pp. 881–886.

[3] A. A. A. Timmermans, R. J. M. Lemmens, M. Monfrance, R. P. J. Geers, W. Bakx, R. J. E. M. Smeets, and H. A. M. Seelen, "Effects of task-oriented robot training on arm function, activity, and quality of life in chronic stroke patients: a randomized controlled trial," *J. NeuroEng. Rehabil.*, vol. 11, p. 45, Mar. 2014.

[4] V. Crocher, K. Brock, J. Simondson, M. Klaic, and M. P. Galea, "Robotic task specific training for upper limb neurorehabilitation: a mixed methods feasibility trial reporting achievable dose," *Disabil. Rehabil.*, pp. 1–9, 2024.

[5] H. Ravichandar, A. S. Polydoros, S. Chernova, and A. Billard, "Recent advances in robot learning from demonstration," *Annu. Rev. Control Robot. Auton. Syst.*, vol. 3, no. Volume 3, 2020, pp. 297–330, 2020.

[6] A. Correia and L. A. Alexandre, "A survey of demonstration learning," *Robot. Auton. Syst.*, vol. 182, p. 104812, 2024.

[7] M. Najafi, K. Adams, and M. Tavakoli, "Robotic learning from demonstration of therapist's time-varying assistance to a patient in trajectory-following tasks," in *2017 International Conference on Rehabilitation Robotics (ICORR)*. IEEE, 2017, pp. 888–894.

[8] B. Luciani, L. Roveda, F. Braghin, A. Pedrocchi, and M. Gandolla, "Trajectory learning by therapists' demonstrations for an upper limb rehabilitation exoskeleton," *IEEE Robot. Autom. Lett.*, vol. 8, no. 8, pp. 4561–4568, 2023.

[9] C. Lauretti, F. Cordella, E. Guglielmelli, and L. Zollo, "Learning by demonstration for planning activities of daily living in rehabilitation and assistive robotics," *IEEE Robot. Autom. Lett.*, vol. 2, no. 3, pp. 1375–1382, 2017.

[10] Z. Liu, Q. Ai, H. Liu, W. Meng, and Q. Liu, "Human-like trajectory planning based on postural synergistic kernelized movement primitives for robot-assisted rehabilitation," *IEEE Trans. Hum.-Mach. Syst.*, 2024.

[11] B. Luciani, S. Costante, F. Braghin, A. Pedrocchi, and M. Gandolla, "Imitation learning using gaussian mixture models and dynamic movement primitives for rehabilitation exoskeletons: A comparison," in *2024 10th IEEE RAS/EMBS International Conference for Biomedical Robotics and Biomechatronics (BioRob)*, 2024, pp. 122–127.

[12] A. Schwarz, J. P. O. Held, and A. R. Luft, "Post-stroke Upper Limb Kinematics of a set of Daily Living Tasks," Mar. 2020.

[13] S. Calinon, "A tutorial on task-parameterized movement learning and retrieval," *Intell. Serv. Robot.*, vol. 9, no. 1, p. 1–29, Jan. 2016.

[14] T. Hastie, R. Tibshirani, J. Friedman, and J. Franklin, "The elements of statistical learning: data mining, inference and prediction," *Math. Intell.*, vol. 27, no. 2, pp. 83–85, 2005.

[15] A. J. Ijspeert, J. Nakanishi, H. Hoffmann, P. Pastor, and S. Schaal, "Dynamical movement primitives: Learning attractor models for motor behaviors," *Neural Comput.*, vol. 25, no. 2, pp. 328–373, 2013.

[16] A. Fabisch, "movement_primitives: Imitation learning of cartesian motion with movement primitives," *Journal of Open Source Software*, vol. 9, no. 97, p. 6695, 2024.

[17] S. Schaal and C. G. Atkeson, "Constructive incremental learning from only local information," *Neural Comput.*, vol. 10, no. 8, p. 2047–2084, Nov. 1998.

[18] T. Flash and N. Hogan, "The coordination of arm movements: an experimentally confirmed mathematical model," *J. Neurosci.*, vol. 5, no. 7, pp. 1688–1703, 1985.

[19] M. Müller, *Information Retrieval for Music and Motion*. Berlin, Heidelberg: Springer-Verlag, 2007.

[20] S. Sempena, N. U. Maulidevi, and P. R. Aryan, "Human action recognition using dynamic time warping," in *Proceedings of the 2011 International Conference on Electrical Engineering and Informatics*, 2011, pp. 1–5.

[21] D. Tolani, A. Goswami, and N. I. Badler, "Real-time inverse kinematics techniques for anthropomorphic limbs," *Graph. Models*, vol. 62, no. 5, pp. 353–388, 2000.

[22] P. F. Lamb and M. Stöckl, "On the use of continuous relative phase: Review of current approaches and outline for a new standard," *Clin. Biomech. (Bristol)*, vol. 29, no. 5, pp. 484–493, Mar. 2014.

[23] A. K. Galgon and P. A. Shewokis, "Using mean absolute relative phase, deviation phase and Point-Estimation relative phase to measure postural coordination in a serial reaching task," *J. Sports. Sci. Med.*, vol. 15, no. 1, pp. 131–141, Feb. 2016.

[24] D. P. Huttenlocher, K. Kedem, and J. M. Kleinberg, "On dynamic voronoi diagrams and the minimum hausdorff distance for point sets under euclidean motion in the plane," in *Proceedings of the Eighth Annual Symposium on Computational Geometry*, ser. SCG '92. New York, NY, USA: Association for Computing Machinery, 1992, p. 110–119.

[25] S. Balasubramanian, A. Melendez-Calderon, A. Roby-Brami, and E. Burdet, "On the analysis of movement smoothness," *J. NeuroEng. Rehabil.*, vol. 12, no. 1, p. 112, Dec. 2015.

[26] M. A. Murphy, C. Willén, and K. S. Sunnerhagen, "Kinematic variables quantifying upper-extremity performance after stroke during reaching and drinking from a glass," *Neurorehabilit. Neural Repair*, vol. 25, no. 1, pp. 71–80, 2011.

[27] R. C. G. Diego Álvarez, Juan C. Alvarez and A. M. López, "Upper limb joint angle measurement in occupational health," *Comput. Methods Biomech. Biomed. Eng.*, vol. 19, no. 2, pp. 159–170, 2016.

[28] J. F. Veale, "Edinburgh handedness inventory–short form: a revised version based on confirmatory factor analysis," *Laterality: Asymmetries of Body, Brain and Cognition*, vol. 19, no. 2, pp. 164–177, 2014.

[29] S. K. Subramanian, J. Yamanaka, G. Chilingaryan, and M. F. Levin, "Validity of movement pattern kinematics as measures of arm motor impairment poststroke," *Stroke*, vol. 41, no. 10, pp. 2303–2308, Sep. 2010.